Light emission and structure of Nd-doped Si-rich-HfO 2 films prepared by magnetron sputtering in different atmospheres

Leonardo Gabriel Vega Macotela, Vega Macotela, Tetyana Torchynska, Larysa Khomenkova, Fabrice Gourbilleau

Light emission and structure of Nd-doped Si-rich-HfO_2 films prepared by magnetron sputtering in different atmospheres

Leonardo Gabriel Vega Macotela[a], Tetyana Torchynska[b,*], Larysa Khomenkova[c,d,e], Fabrice Gourbilleau[d]

[a] *Instituto Politécnico Nacional - ESIME, México City, 07738, Mexico*
[b] *Instituto Politécnico Nacional - ESFM, México City, 07738, Mexico*
[c] *V. Lashkaryov Institute of Semiconductor Physics at the NAS of Ukraine, 45 pr. Nauky, Kyiv, 03028, Ukraine*
[d] *CIMAP, UMR CNRS/CEA/ENSICAEN/UNICAEN, 6 Boulevard Maréchal Juin, 14050, Caen Cedex 4, France*
[e] *National University "Kyiv-Mohyla Academy", 2 Skovorody str., Kyiv, 04170, Ukraine*

A B S T R A C T

Radio-frequency magnetron sputtering was used to produce HfO_2 films doped with Nd, Si and N. The deposition was carried out in two different atmospheres: i) in pure argon plasma to grow Si-HfO_2:Nd films, and ii) in argon-nitrogen mixed plasma to produce Si-N-HfO_2:Nd films. The effect of annealing temperature on optical and structural properties of the films was investigated. Annealing was performed at T_A = 800–1100 °C for t_A = 15 min in nitrogen atmosphere. The evolution of film's properties was studied by means of the scanning electronic microscopy (SEM), energy dispersive X-ray spectroscopy (EDS), X-ray diffraction (XRD) and photoluminescence (PL) methods. It was observed that the film morphology depends significantly on the deposition atmosphere. For the Si-HfO_2:Nd films, the presence of the grains with the mean size about 100 nm was detected by the SEM method. The tetragonal HfO_2 and SiO_2 phases have been detected by the XRD method after film annealing at 950 °C. PL spectra of these films are complex and demonstrate several PL bands in the visible (400–750 nm) and infrared (800–1430 nm) spectral ranges. Their contribution depends on the annealing temperature and governs the shape of total PL spectrum. In contrary, the Si-N-HfO_2:Nd films showed unstructured smooth surface as well as featureless PL spectra. Whatever the annealing temperature, they demonstrate broad unstructured PL band with the peak within 440–480 nm. Peculiarities of PL spectra of both types of the films and the mechanism of phase separation are analyzed and discussed.

* Corresponding author.
E-mail address: ttorch@esfm.ipn.mx (T. Torchynska).

1. Introduction

HfO_2-based materials during the last decades are mainly considered as the alternative gate dielectrics to silicon oxide in complementary metal-oxide semiconductor technology. At the same time, their high refractive index (n = 1.9–2.2, depending on preparation method), high optical transparency in the ultraviolet-infrared spectral range (band gap is about 5.8–6.0 eV), compactness and hardness offer optical applications as well. The phonon cut-off energy (~about 780 cm^{-1}) reduces the probability of non-radiative phonon assisted relaxation that is attractive for doping these materials in particular with the rare-earth elements [1–3]. However, in spite of mentioned advantages, the HfO_2-based compounds up to now are not often addressed as a host for the rare-earth ions. Just a few groups reported on the light emission obtained from Eu^{3+}-doped HfO_2-based nanotubes [4], Er^{3+}-doped sol-gel SiO_2-HfO_2 waveguides [5–7], as well as Er^{3+} or Pr^{3+} doped HfO_2-based thin films [8,9].

Among different rare-earth ions, the trivalent neodymium (Nd^{3+}) was used in the inorganic laser materials attracting the great attention of scientific researches and industrial applications. Nd^{3+} ions exhibit broad and strong absorption band around 800 nm and a very intense emission in the near-infrared luminescence range from 800 to 1430 nm associated with the $^4F_{3/2} \rightarrow {}^4I_J$ (J = 9/2, 11/2, 13/2) optical transitions in the 4*f* inner electronic shell of Nd^{3+} ions, following a known "four-level" scheme [10,11]. The $^4F_{3/2}$ emitting state can be populated conveniently by the emission of low-cost commercially available laser diodes. In addition, it has many intense pumping levels and efficient up-converted emissions [11]. Among different host matrix materials, the garnets [10], glasses [12], ceramics [13], II-VI compounds [14], as well as Si-rich SiO_2 or Si_3N_4 are the most studied [15,16].

In this work we present the results of the structural and spectroscopic study of HfO_2-based thin films co-doped with Si, N and Nd grown by radio frequency (RF) magnetron sputtering. The effect of annealing temperature on the phase separation process and luminescence of such composite films is considered as a fruitful way for monitoring the properties of these materials.

2. Experimental details

The films were grown by RF magnetron sputtering on 2-inch, B-doped, (100) oriented Si wafers with a resistivity of about 15 Ω cm. Prior to the deposition, the substrates were submitted to standard RCA cleaning: dipped in a diluted hydrofluoric solution (10%), dried in N_2, and immediately transferred to the load-lock vacuum chamber of the deposition setup. A pure HfO_2 target (99.9%) topped with the calibrated Si and Nd_2O_3 pellets was used. The Si and Nd_2O_3 pellets covered about 16% of target surface each.

To produce the Si-HfO_2:Nd films, the deposition was performed in pure Ar plasma with argon flow f_{Ar} = 3sccm (so-called "standard" approach). The deposition time was 200 min allowed to grow homogeneous film with the thickness of about 410 nm.

The Si-N-HfO_2:Nd films were produced with Ar-N_2 mixed plasma (f_{Ar} = 3 sccm and f_{N2} = 2 sccm; so-called "reactive" approach). The deposition time was 240 min resulting in the film thickness of about 260 nm.

All other deposition conditions were similar for both approaches, i.e. the RF power density, substrate temperature (T_S), total plasma pressure and substrate-cathode distance were 0.74 W/cm^2, 400 °C, 0.03 mbar and 57 mm, respectively. After the film deposition, each substrate was cut onto the smaller pieces (usually 1 × 1 cm^2) to study the effect of annealing treatment. It was performed in a conventional horizontal furnace at different temperatures T_A = 800–1100 °C during t_A = 15 min in a continuous nitrogen flow (f_{N2} = 48 sccm).

Several experimental techniques were used to analyze the properties of the films. The PL emission was excited with a 325 nm line of He-Cd laser or by different lines of Ar^+-ion laser. PL spectra were recorded using several setups: i) a Jobin–Yvon TRIAX 180 monochromator linked with a fast Hamamatsu photomultiplier and a SRS lock-in amplifier (SP830 DPS) (for 400–1000 nm spectral range); ii) with a Jobin Yvon 1 m single grating monochromator coupled to a Northcoast Germanium detector cooled with liquid nitrogen and a SRS lock-in amplifier (SP830 DPS) (for 800–1700 nm spectral range). Referenced chopping frequency was 20 Hz.

To study the film surface morphology as well as to get the information on their chemical composition, a scanning electronic microscope (SEM) Quanta 3D FEG-FEI with an additional detector Apollo X10 mark EDAX for the energy dispersive X-ray spectroscopy (EDS) was used.

X-ray diffraction (XRD) results were obtained using the equipment of Model X'PERT MRD with the Pixel detector, three-axis goniometry and parallel collimator with the angular resolution of 0.0001°. X-ray beam was achieved from the Cu source ($K_{\alpha 1}$ line, λ = 1.5406 Å). All experiments were carried out at the room temperature.

3. Results and discussion

3.1. Chemical composition of the films

The chemical composition of the films was analyzed by energy-dispersive X-ray spectroscopy (EDS). The representative spectra for as-deposited films are shown in Fig. 1. As one can see, for all films, the presence of Hf, Si, O and Nd elements was registered. In addition, for the films deposited in argon-nitrogen plasma, the significant signal from the nitrogen was also detected (Fig. 1a, curve 2). Note that the carbon signal can be due to the carbon adsorption on the film surface from an ambient atmosphere.

The annealing treatment results in the variation of chemical composition of the samples that is more prominent for the Si-N-HfO_2:Nd films. It turned out that the nitrogen-related signal is the most affected. Its intensity changes slightly for T_A < 950 °C (not shown) and decreases significantly for higher temperatures (T_A = 1000–1100 °C)

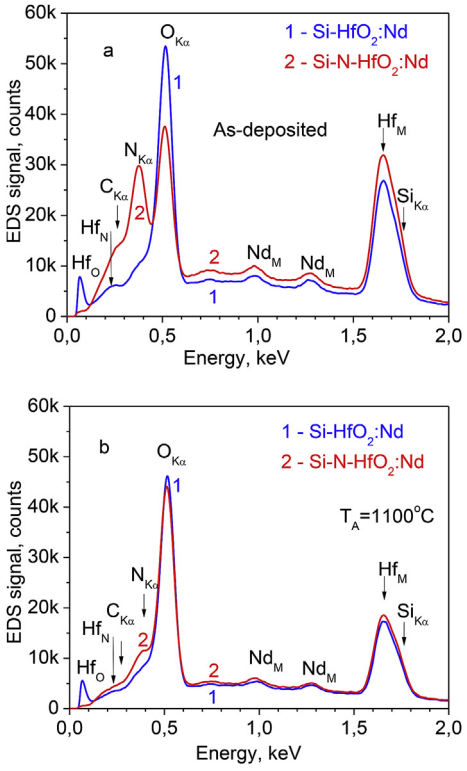

Fig. 1. EDS spectra for Si-HfO_2:Nd (curves 1) and Si-N-HfO_2:Nd (curves 2) films, as-deposited (a) and annealed at 1100 °C (b).

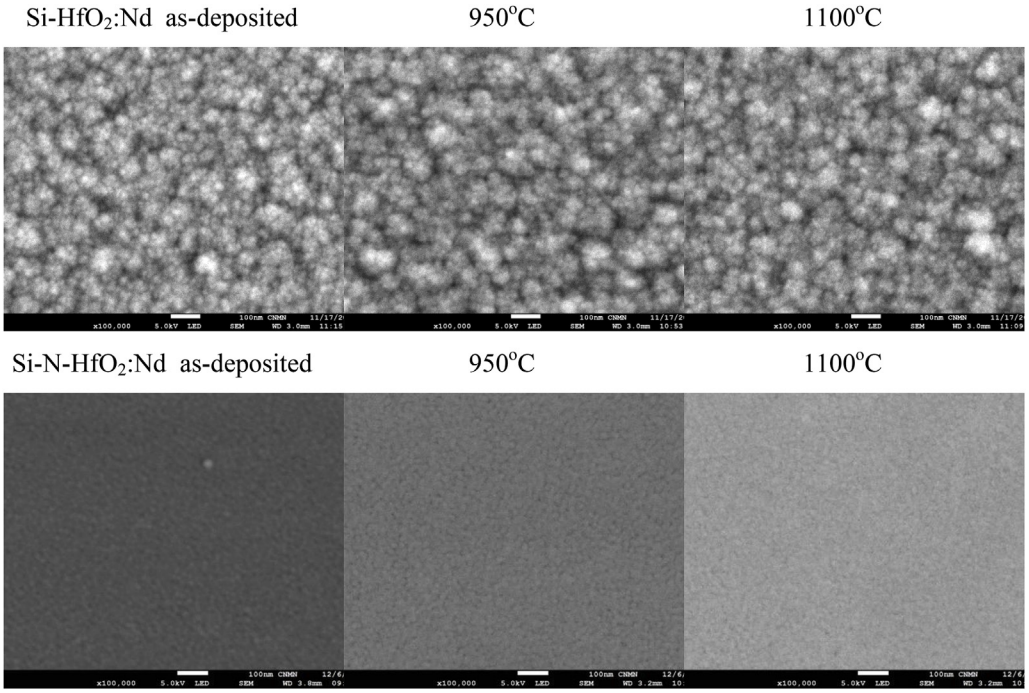

Fig. 2. Surface SEM images of the Si-HfO_2:Nd (upper panel) and Si-N-HfO_2:Nd (bottom panel) films as-deposited and annealed at 950 and 1100 °C.

(Fig. 1b). This effect can be explained taking into account the results of Ref. [17]. The authors demonstrated that rapid (60 s) thermal annealing at 1000 °C in nitrogen atmosphere of HfSiON thin films causes the O and N atomic transport and exchange of the chemical species resulting either in the Si-N or Si-O-N bond formation, as well as in the NO formation and its out-diffusion from the samples. Considering the annealing conditions used for our Si-N-HfO_2:Nd films, one can assume that the similar processes can occur in our films. Since the N-related EDS signal decreases in intensity, one can conclude that NO formation is the main process for the N desorption from the films. It should be noted that EDS spectra of annealed Si-HfO_2:Nd films were found to be similar to those of as-deposited ones.

3.2. Surface morphology

Fig. 2 represents the surface SEM images of the Si-HfO_2:Nd (Fig. 2, upper panel) and Si-N-HfO_2:Nd (Fig. 2, bottom panel) samples. As one can see, the morphology of as-deposited films depends very much on the sputtering approach. The Si-N-HfO_2:Nd films, grown with reactive approach, show smooth surface contrary to their Si-HfO_2:Nd counterparts deposited in pure argon plasma (Fig. 2). This difference in the film morphology can be explained taking into account the structure zone model (SZM) proposed in 1969 for the films grown by electron-beam plasma vapor deposition [18] and developed later for the sputtering approach [19].

The real structure of the film is determined by four processes: i) shadowing, i.e. a geometric interaction between arriving adatoms and the roughness of the growing surface; ii) surface diffusion, i.e. mobility of adatoms at the surface and interfaces such as grain boundaries; iii) bulk diffusion, i.e. mobility of adatoms in the volume of grains, and iv) recrystallization, i.e. phase transition as a complete change of crystal orientation [18,19]. The processes i) and ii) dominate at low and medium temperature of the substrate, T_S, respectively. Processes iii) and iv) are important at high T_S. Besides, process iv) dominates at the percolation thickness and large film thickness.

It was shown that for the most metals and dielectrics, activation energies for diffusion are related to the melting temperature of material, T_M [18]. Thus, the basic processes depend on the T_S/T_M ratio and determine the final structure of the film. In the regard of the value of T_S/T_M ratio, three different zones were considered: i) when $T_S/T_M < 0.3$, the formation of fine-grained porous structure due to the low mobility of adatoms and their stick at the place, where they were land on the substrate (zone I); ii) when $0.3 < T_S/T_M < 0.5$, a columnar structure grows owing to surface diffusion of adatoms with the activation energy of 0.1–0.3 eV (zone II); iii) for $T_S/T_M > 0.5$, a rough equiaxed grain structure appears due to the high bulk diffusion with the activation energy of above 0.3 eV (zone III) [18].

Later, in this model the effect of the total plasma pressure on the film structure was introduced [19]. It was shown that for $T_S/T_M < 0.1$ and a higher argon pressure the formation of porous structure is less probable due to the high deposition rate (10 nm/min) and limited adatom surface mobility. At the same time for $T_S/T_M = 0.1$–0.3 (so-called after zone T), the self-diffusion is appreciable and the formation of films with the dense array of grains separated by grain boundaries occurs owing to sintering the grains. However, for $T_S/T_M > 0.3$, the effect of argon pressure decreases significantly with T_S/T_M rise and the real film structure can be found to be similar to that proposed in Ref. [18].

Taking into account the substrate temperature (T_S = 400 °C) used for the fabrication of the films investigated and the melting temperature of sputtered targets, the T_S/T_M ratio can be determined. However, the melting temperature of the target can be roughly estimated. This target was constructed as the HfO_2 target (T_M = 2810 °C) topped with Si (T_M = 1410 °C) and Nd_2O_3 (T_M = 2233 °C) pellets. However, the main contribution in sputtering was given by the HfO_2 target. Considering corresponding T_M values, one can obtain the $T_S/T_M \sim 0.14$ that is corresponding to the zone T in the SZM model. One can expect the formation of the grain dense arrays separated with the grain boundaries. The surface of the films should show the presence of grains or clusters of different heights. This structure was found for the as-deposited Si-HfO_2:Nd films (Fig. 2, upper panel). They contain the nanocrystal grains with the mean size of about 20–60 nm. These films show developed structure, i.e. the nanocrystals form the micro-clusters separated by the valleys.

For the films grown with reactive approach, the effect of nitrogen addition has to be taken into account. In this case the total plasma

pressure was kept to be the same as for a standard approach. However, the nitrogen incorporation in the plasma implies on the change in the plasma dynamics because N_2 number increasing leads to enlarging the collision probability of atoms with the substrate surface and promotes a larger number of chemical reactions. The collisions enhances the atom surface mobility and increasingly smooth the film by the surface diffusion [20].

Recently, the effect of the oxygen content on the structure of SnO-SnO_2-Sb_2O_3 films was considered in Ref. [21]. It was reported decreasing the grain size and film roughness due to the high particle collision, enhanced atom surface diffusion and surface atom mobility in the growing films. This effect becomes more prominent for the higher oxygen content. For the film grown with $O_2/Ar = 0.47$ the formation of very smooth films with small grains was found. Considering the mentioned above findings, one can explain the difference in the morphology of Si-HfO_2:Nd and Si-N-HfO_2:Nd films. For the latter the higher probability of particle collisions with the surface of growing film and higher diffusion of adatoms allows to form a surface covering layer and to block the grain's growth. This leads to the repeated nucleation and the formation of smooth films.

The annealing treatments at 950 and 1100 °C results in increasing the grain sizes in the Si-HfO_2:Nd films up to 40–100 nm due to the change of grain boundaries and the coalescence of small grains (Fig. 2). Annealing the Si-N-HfO_2:Nd samples does not affect their surface structure very much. However, the films annealed at $T_A = 1100$ °C demonstrate some tendency in their densification (Fig. 2). It is worth to point that the more prominent effect on the film structure is appeared from the deposition conditions. The use of reactive approach allows the fabrication of smoother films.

3.3. XRD study

The samples described above were characterized by the XRD method. XRD patterns recorded with the symmetric geometry are shown in Fig. 3a, b. The both types of studied films in as-deposited states demonstrate a series of XRD peaks that can be attributed to the different phases. The very intensive two XRD peaks at 32.9726° (Figs. 3b) and 69.0523° (Fig. 3a and b) were identified as the XRD signal of the Si substrates, i.e. from (112) and (400) planes in cubic Si crystal lattice (Table 1). Additionally, a set of XRD peaks with the low intensity (Table 1) was assigned to the X-ray diffraction in the tetragonal $Nd_2Si_2O_7$ and tetragonal $HfSiO_4$ phases (Table 1). These phases were supposed to be appeared in the film due to the high deposition temperature of 400 °C.

Table 1
XRD peaks in as-deposited Si-HfO_2:Nd and Si-N-HfO_2:Nd films.

Peak	Degree	(h k l)	Phase	Crystal type	ICSD
a	32.9726	(1 1 2)	Si	Cubic	00-005-0490
a*	34.0723	(2 1 1)	$HfSiO_4$	Tetragonal	01-077-1759
b	55.8723	(4 0 0)	$HfSiO_4$	Tetragonal	01-077-1759
c	61.6237	(2 4 1)	$Nd_2Si_2O_7$	Tetragonal	01-089-5347
d	66.2150	(3 3 8)	$Nd_2Si_2O_7$	Tetragonal	01-089-5347
e	69.0523	(4 0 0)	Si	Cubic	00-005-0490
e*	69.8360	(3 2 3)	$HfSiO_4$	Tetragonal	01-077-1759
e"	73.6440	(4 3 1)	$HfSiO_4$	Tetragonal	01-077-1759

Table 2
XRD peaks of Si-HfO_2:Nd film annealed at 950 °C (Fig.3a).

Peak	Degree	(h k l)	Phase	Crystal type	ICSD
1a	30.0643	(1 0 1)	HfO_2	Tetragonal	00-008-0342
1b	30.1870	(1 1 0)	SiO_2	Tetragonal	00-045-1374
1c	30.7750	(1 0 1)	Nd_2O_3	Hexagonal	00-041-1089
2a	34.1623	(0 0 2)	HfO_2	Tetragonal	00-008-0342
2b	35.1123	(2 0 0)	HfO_2	Tetragonal	00-008-0342
3a	49.9123	(2 0 2)	HfO_2	Tetragonal	00-008-0342
3b	50.2723	(2 2 0)	HfO_2	Tetragonal	00-008-0342
4a	59.7523	(3 1 1)	HfO_2	Tetragonal	00-008-0342
4b	59.9723	(2 2 2)	HfO_2	Tetragona	00-008-0342
4c	60.4242	(1 2 1)	SiO_2	Tetragonal	00-045-1374
5	69.0523	(4 0 0)	Si	Cubic	00-005-0490
6	82.1823	(2 0 4)	HfO_2	Tetragonal	00-008-0342

The thermal treatment of the Si-HfO_2:Nd film at $T_A = 950$ °C leads to the significant changes of XRD patterns. The signal from the tetragonal $Nd_2Si_2O_7$ and tetragonal $HfSiO_4$ phases disappeared, while the XRD peaks related to the tetragonal HfO_2 phase become significant (Fig. 3a, Table 2). The intensities of five XRD peaks related to this phase (Fig. 3a, the peaks denoted as 1, 2, 3, 4, 6) increased significantly (Fig. 3a). Additionally, the XRD signal of the cubic Si phase (peak 5) and new XRD peaks, identified as the X-ray diffraction from the crystal planes in the hexagonal Nd_2O_3 (peak 1c) and tetragonal SiO_2 (peak 1b) lattices, were detected (Fig. 3a, Table 2). Simultaneously, the improved crystallinity of the Si-HfO_2:Nd film annealed at $T_A = 950$ °C hampers the detection of XRD peaks from underlying Si substrate (Fig. 3a).

Thermal annealing the Si-N-HfO_2:Nd films is less effective. The crystallization process in these films at $T_A = 950$ °C is completely different (Fig. 3b). All XRD peaks, which were revealed in the as-deposited Si-N-HfO_2:Nd film, have been detected also after their annealing at

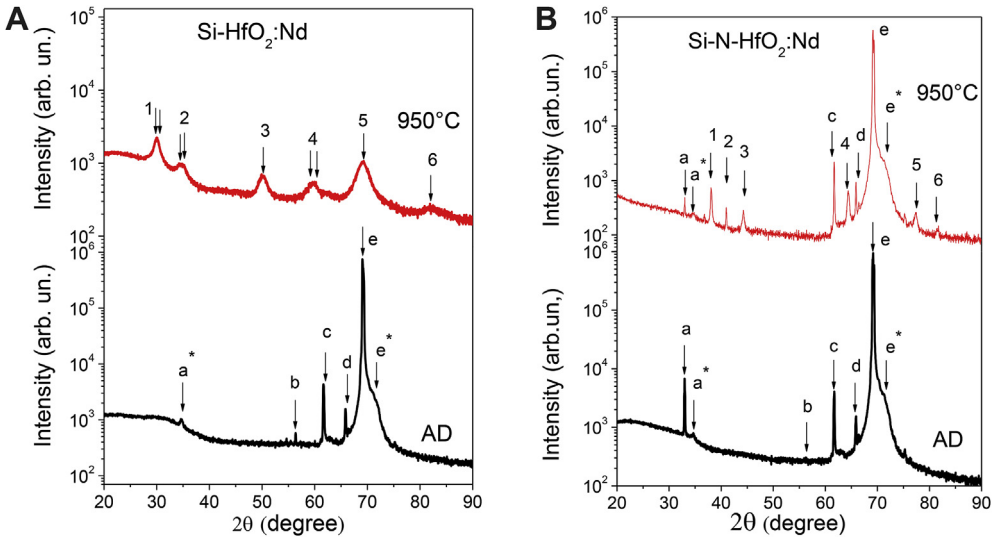

Fig. 3. XRD spectra for Si-HfO_2: Nd (a) and Si-N-HfO_2: Nd (b) films, as-deposited and annealed at 950 °C.

Table 3
XRD peaks of Si-N-HfO_2:Nd film annealed at 950 °C (Fig.3b).

Peak	Degree	(h k l)	Phase	Crystal type	ICSD
a	33.0126	(1 1 2)	Si	Cubic	00-005-0490
a*	34.0723	(2 1 1)	$HfSiO_4$	Tetragonal	01-077-1759
1	38.6826	(2 2 0)	$HfSiO_4$	Tetragonal	01-077-1759
2	40.7726	(2 0 2)	$HfSiO_4$	Tetragonal	01-077-1759
3	44.0526	(3 0 1)	$HfSiO_4$	Tetragonal	01-077-1759
c	61.6237	(2 4 1)	$Nd_2Si_2O_7$	Tetragonal	01-089-5347
4	64.6307	(4 0 2)	$HfSiO_4$	Tetragonal	01-077-1759
d	66.2150	(3 3 8)	$Nd_2Si_2O_7$	Tetragonal	01-089-5347
e	69.0523	(4 0 0)	Si	Cubic	00-005-0490
e*	69.8360	(3 2 3)	$HfSiO_4$	Tetragonal	01-077-1759
e*	73.6440	(4 3 1)	$HfSiO_4$	Tetragonal	01-077-1759
5	76.4726	(4 1 3)	$HfSiO_4$	Tetragonal	01-077-1759
6	81.1056	(5 1 2]	$HfSiO_4$	Tetragonal	01-077-1759

950 °C (Fig. 3b). Additionally, the new XRD peaks (Fig. 3b, peaks 1–6) have appeared and were attributed to the tetragonal $HfSiO_4$ phase (Table 3). Note that owing to the less effective crystallization process in the Si-N-HfO_2:Nd film at 950 °C, the peaks related to the XRD in the Si substrate can be still detected in the XRD pattern (Fig. 3b).

3.4. Light-emitting properties

The luminescent spectroscopy is a powerful tool for the characterization of rare-earth doped materials. Hereafter the most interesting results for the films described above will be presented. Note that the majority researchers were focused early on the investigation of the near-infrared PL spectrum in the range 800–1400 nm [10–16]. Typical radiative emission bands of Nd^{3+} ions in the mentioned range can be detected at 880, 1060, and 1350 nm [10,22–24]. These emission bands originate from the electronic transitions between $4f^N$ levels: $^4F_{3/2} \rightarrow {}^4I_{9/2}$, $^4F_{3/2} \rightarrow {}^4I_{11/2}$ and $^4F_{3/2} \rightarrow {}^4I_{13/2}$ in Nd^{3+} ions (Table 4).

It is essential that the high PL intensity in the studied films was detected for the annealed films. The spectra registered in the visible and IR spectral ranges with the excitation by the 325 nm line of a He-Cd laser and 488 nm line of an Ar^+ -ion lasers are shown in Fig. 4 and Fig. 5a, respectively. The total PL intensity has non-monotonic behavior with annealing temperature. The highest PL intensity was detected for the films annealed at T_A = 900–950 °C whatever the deposition approaches.

Fig. 4a shows the visible PL spectra of the Si-HfO_2:Nd films in the as-deposited state and after annealing at T_A = 950 °C. As one can see, the PL spectrum consists the several PL components related to the optical transitions in the 4f inner electronic shell of Nd^{3+} ions with a set of peaks in the spectral range of 350–900 nm (Table 4). Their contribution depends on the annealing temperature and governs the shape of total PL spectrum. The crystallization of the Si-HfO_2:Nd film upon annealing at 950 °C and the appearance of the tetragonal HfO_2 crystal phase (Table 2) lead to significant increasing the PL intensity of visible and IR

Table 4
Optical transitions detected in Si-HfO_2:Nd films (Fig. 4a).

Number	Wavelength, nm	Optical transition	Reference
1	400	$^4P_{1/2} \rightarrow {}^4I_{9/2}$	[14]
2	455	$^4G_{11/2} \rightarrow {}^4I_{9/2}$	[=23,24]
3	540–550	$^4G_{7/2} \rightarrow {}^4I_{9/2}$	[12,24]
4	560	$^4G_{5/2} \rightarrow {}^4I_{9/2}$	[12,22]
5	660	$^4F_{9/2} \rightarrow {}^4I_{9/2}$	[10]
5	650	$^2G_{7/2} \rightarrow {}^4I_{9/2}$	[24]
6	710	$^4F_{7/2} \rightarrow {}^4I_{9/2}$	[24]
7	790	$^2H_{9/2}, {}^4F_{5/2} \rightarrow {}^4I_{9/2}$	[22]
8	880	$^4F_{3/2} \rightarrow {}^4I_{9/2}$	[10]
9	1074	$^4F_{3/2} \rightarrow {}^4I_{11/2}$	[10]
10	1330	$^4F_{3/2} \rightarrow {}^4I_{13/2}$	[10]

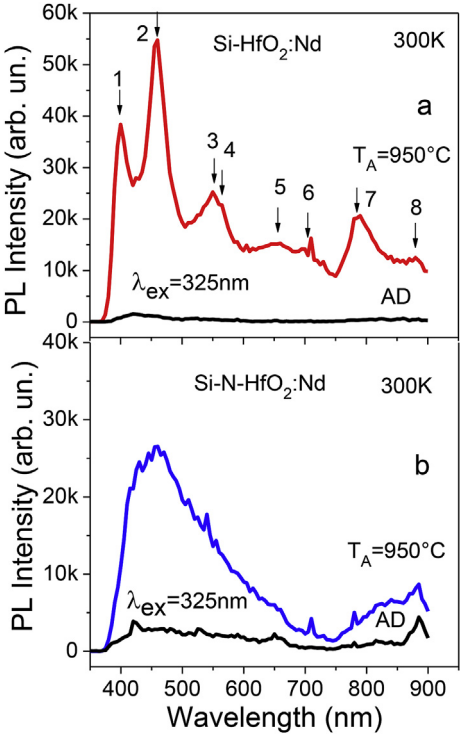

Fig. 4. PL spectra for Si-HfO_2: Nd (a) and Si-N-HfO_2: Nd (b) films, as-deposited and annealed at 950 °C, detected by a photo multiplayer tube.

PL bands (Table 4, Fig. 6).

In contrary, the PL spectra of the Si-N-HfO_2:Nd film are still featureless after annealing at T_A = 950 °C (Fig. 4b). Actually, the PL intensity increases after annealing, but whatever the annealing temperatures, PL spectra demonstrate broad unstructured PL bands with the main peak within 440–480 nm and other small PL peaks in the range of 750–900 nm (Fig. 4b). Thus the less effective crystallization of the Si-N-HfO_2:Nd film upon annealing (Fig. 3b) no permit re-arranging the Nd^{3+} ions in host matrix that is necessary to obtain the efficient radiative defects.

Fig. 5a represents the PL spectra of both films in the range of 800–1400 nm. One can see that the typical radiative emission bands of Nd^{3+} ions are detected at 880, 1060, and 1350 nm. The spectra have similar shape. The difference in the intensity can be explain by the less effective crystallization of the Si-N-HfO2:Nd film upon annealing and lower amount of the sensitizers in Si-N-HfO_2:Nd that can excite the Nd^{3+} ions. Another reason can be the competition between different radiative channels contributed in the visible broad PL band.

The effect of the excitation wavelengths on the intensity of PL bands centered at 550 nm and 880 nm is shown in Fig. 5b for the Si-HfO_2:Nd film. As one can see, the PL bands at 550 nm and 880 nm have the similar PL intensities under the excitation with the 500 nm and 514 nm light wavelengths. However, at shorter excitation wavelengths, the 880-nm Nd^{3+} PL band demonstrates some kind of saturation, whereas the 550-nm PL bands increases in the intensity. It is worth to point that 476 and 455 nm excitation is the non-resonant and resonant excitations for the Nd^{3+} ions, respectively (Table 4). The similar intensities of the 880-nm Nd^{3+} PL band related to the $^4F_{3/2} \rightarrow {}^4I_J$ (J = 9/2) radiative transition detected at the both excitations (resonant and non-resonant) give the evidence that the rare-earth ions are excited via energy transfer from the Si nanoclusters or host defects as well. Recently we have demonstrated such effect for the Er-doped and Pr-doped HfSiO films [8,9].

The increase of annealing temperatures results in decreasing the PL intensity of Nd-related PL bands in the both types of investigated films. This can be due to the formation of Nd-oxide or Si-oxide phases, as well as due to decreasing the number of sensitizers, for instance, the Si

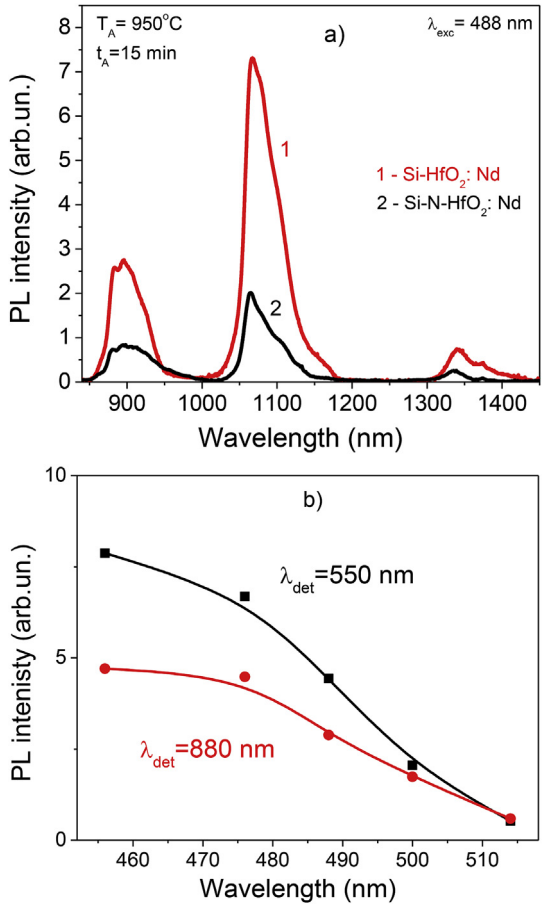

Fig. 5. a) PL spectrum of the Si-HfO$_2$: Nd (1) and Si-N-HfO$_2$:Nd (2) films annealed at 950 °C in the range 850–1500 nm. The spectra are normalized for the film thickness. The excitation wavelength is 488 nm (non-resonant for Nd^{3+} ions). b) Variation of PL intensity for the PL peaks at 550 nm and 880 nm versus excitation wavelength detected in the Si-HfO$_2$: Nd film annealed at 950 °C.

nanoclusters, caused by their oxidation, or recovering the host defects.

4. Conclusions

In the present work, the effects of deposition and annealing conditions on the emission, chemical composition and structural properties of the Si-HfO$_2$:Nd and Si-N-HfO$_2$:Nd films have been studied. The Nd-related emission was achieved via the direct excitation of the ions as well as by the excitation via Si-nanoclusters. It is also demonstrated that in the film grown in pure argon plasma, the formation of the nanocrystal tetragonal HfO$_2$ phase upon high-temperature annealing favors the bright emission related to the optical transitions via the 4f inner electronic levels in Nd^{3+} ions. Using the argon-nitrogen plasma allows the fabrication of films with the same composition, but the smooth surface that may be interesting for optic waveguide applications. The annealing of these films is less efficient in terms of the film crystallization. It was shown that the highest Nd-related PL emission can be obtained from the films heat treated at 900–950 °C.

Acknowledgements

This work was partly supported by National Academy of Sciences of Ukraine (project III-4-16), Ministry of Education and Science (project ID: 89452), the French National Agency of Research (ANR), as well as by the CONACYT Mexico (project 258224) and SIP, IPN Mexico (project 20180495).

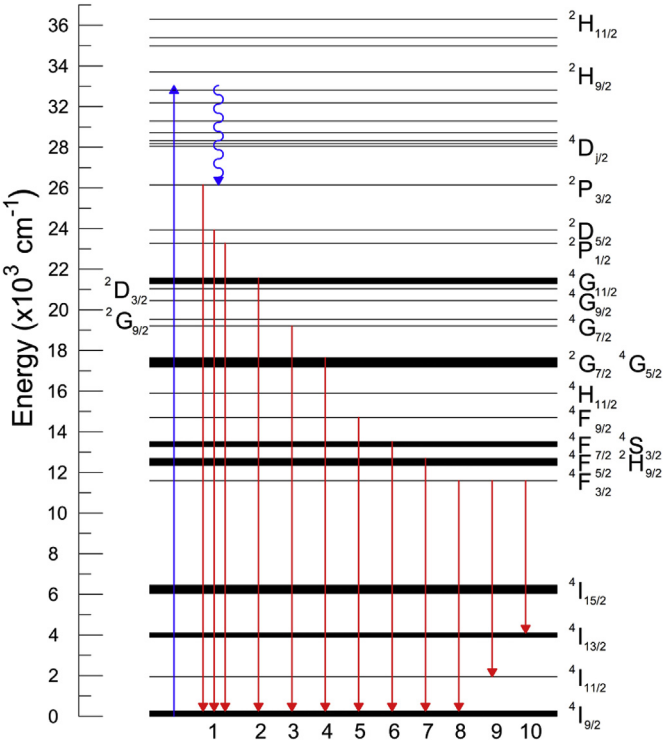

Fig. 6. Excitation and recombination optical transitions via the 4f inner electronic levels detected for the Nd^{3+} ions embedded in Si-HfO$_2$:Nd films. The Nd^{3+} energy level diagram was taken from Ref. [11].

References

[1] M. Park, T. Schenk, C.M. Fancher, E.D. Grimley, C. Zhou, C. Richter, L.M. LeBeau, J.L. Jones, T. Mikolajick, U. Schroder, J. Mater. Chem. C 5 (2017) 4677.
[2] S. Starschich, T. Schenk, U. Schroder, U. Boettger, Appl. Phys. Lett. 110 (2017) 182905.
[3] M.H. Park, T. Schenk, M. Hoffmann, S. Knebel, J. Gartner, T. Mikolajick, U. Schroder, Nanomater. Energy 36 (2017) 381.
[4] L.X. Liu, Z.W. Ma, Y.Z. Xie, Y.R. Su, H.T. Zhao, M. Zhou, J.Y. Zhou, J. Li, E.Q. Xie, J. Appl. Phys. 107 (2010) 024309.
[5] G.C. Righini, S. Berneschi, G. Nunzi Conti, S. Pelli, E. Moser, R. Retoux, P. Féron, R.R. Gonçalves, G. Speranza, Y. Jestin, M. Ferrari, A. Chiasera, A. Chiappini, C. Armellini, J. Non-Cryst. Sol. 355 (2009) 1853–1860.
[6] N.D. Afify, G. Dalba, F. Rocca, J. Phys. D Appl. Phys. 42 (2009) 115416.
[7] L. Minati, G. Speranza, V. Micheli, M. Ferrari, Y. Jestin, J. Phys. D Appl. Phys. 42 (2009) 015408.
[8] L. Khomenkova, Y.-T. An, D. Khomenkov, X. Portier, C. Labbé, F. Gourbilleau, Phys. B Condens. Matter 453 (2014) 100–106.
[9] R. Demoulin, G. Beainy, C. Castro, P. Pareige, L. Khomenkova, C. Labbé, F. Gourbilleau, E. Talbot, Nano Futures 2 (2018) 035005.
[10] V. Monteseguro, M. Rathaiah, K. Linganna, A.D. Lozano-Gorrín, M.A. Hernández-Rodríguez, I.R. Martín, P. Babu, U.R. Rodríguez-Mendoza, F.J. Manjón, A. Muñoz, C.K. Jayasankar, V. Venkatramu, V. Lavín, Opt. Mater. Express 5 (2015) 1661.
[11] M. Pollnau, P.J. Hardman, W.A. Clarkson, D.C. Hanna, Optic Commun. 147 (1998) 203.
[12] E.O. Serqueira, N.O. Dantas, Optic Lett. 39 (2014) 131.
[13] G. Yi, W. Li, J. Song, B. Mei, Z. Zhou, L. Su, J. Eur. Ceram. Soc. 38 (2018) 3240.
[14] M. Balestrieri, S. Colis, M. Gallart, G. Ferblantier, D. Muller, P. Gilliot, P. Bazylewski, G.S. Chang, A. Slaouib, A. Dinia, J. Mater. Chem. C 2 (2014) 9182.
[15] C.-H. Liang, O. Debieu, Y.-T. An, L. Khomenkova, J. Cardin, F. Gourbilleau, J. Lumin. 132 (2012) 3118.
[16] P. Pirasteh, J. Charrier, Y. Dumeige, J.-L. Doualan, P. Camy, O. Debieu, Ch-H. Liang, L. Khomenkova, J. Lemaitre, Y.G. Boucher, F. Gourbilleau, J. Appl. Phys. 114 (2013) 014906.
[17] L. Miotti, K.P. Bastos, G.V. Soar, C. Driemeier, R.P. Pezzi, J. Morais, I.J.R. Baumvol, A.L.P. Rotondaro, M.R. Visokay, J.J. Chambers, M. Quevedo-Lopez, L. Appl. Phys. Lett. 85 (2004) 4460.
[18] B.A. Movchan, A.V. Demchishin, Fiz. Metal. Metalloved. 28 (1969) 653.
[19] J.A. Thornton, J. Vac. Sci. Technol. 11 (1974) 666.
[20] P.B. Barna, A. Adamik, Thin Solid Films 317 (1998) 27.
[21] S.-S. Lin, C.-K. Peng, C.-W. Li, J. Alloy. Comp. 770 (2019) 433.
[22] J. Cui, G.A. Hope, Raman and fluorescence spectroscopy of CeO_2, Er_2O_3, Nd_2O_3, Tm_2O_3, Yb_2O_3, La_2O3, and Tb_4O_7, J. Spectroscopy (2015) 8 V. 2015, ID 940172 https://doi.org/10.1155/2015/940172.
[23] L. Liu, M. Li, Sh Cai, Y. Yang, Y. Mai, Opt. Mater. Express 5 (2015) 756.
[24] T. Som, B. Karmakar, J. Alloy. Comp. 476 (2009) 383.